

KERNFORSCHUNGSZENTRUM

KARLSRUHE

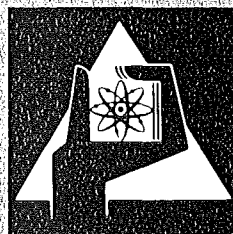
Mai 1977

KFK 2455

Institut für Angewandte Kernphysik

**Alpha-Gamma Angular Correlations
in the Reaction $^{24}\text{Mg}(\alpha, \alpha_1\gamma)$ at $E_\alpha = 104 \text{ MeV}$**

W. Eyrich, A. Hofmann, U. Scheib,
S. Schneider, F. Vogler, H. Rebel



**GESELLSCHAFT
FÜR
KERNFORSCHUNG M.B.H.**

KARLSRUHE

Als Manuskript vervielfältigt

Für diesen Bericht behalten wir uns alle Rechte vor

GESELLSCHAFT FÜR KERNFORSCHUNG M. B. H.
KARLSRUHE

KERNFORSCHUNGSZENTRUM KARLSRUHE

KFK 2455

Institut für Angewandte Kernphysik

ALPHA-GAMMA ANGULAR CORRELATIONS
IN THE REACTION $^{24}\text{Mg}(\alpha, \alpha_1\gamma)$ AT $E_\alpha = 104$ MeV

W. Eyrich⁺, A. Hofmann⁺, U. Scheib⁺, S. Schneider⁺ and F. Vogler⁺

and

H. Rebel

⁺ Physikalisches Institut der Universität Erlangen-Nürnberg, Erlangen

Gesellschaft für Kernforschung mbH, Karlsruhe

Abstract

The in-plane α_1 - γ angular correlation of the reaction $^{24}\text{Mg}(\alpha, \alpha'\gamma)$ has been studied at a bombarding energy of 104 MeV. Double differential cross sections have been measured for 126 pairs of angles by use of a multidetector arrangement consisting of four Si(Li) particle detectors and two Ge(Li) γ -detectors. The correlation data are described very well by coupled channel calculations on the basis of a symmetric rotator model. A strong sensitivity to the sign of the quadrupole deformation has been found. This sensitivity proves to be nearly independent of the potential parameters. The main features of the observed prolate-oblate effects can be understood in the framework of a simple diffraction model.

ALPHA-GAMMA KORRELATIONEN IN DER REAKTION $^{24}\text{Mg}(\alpha, \alpha_1\gamma)$ BEI $E_{\alpha} = 104$ MeV

Zusammenfassung

Bei einer Einschussenergie von $E_{\alpha} = 104$ MeV wurde die "in plane" α_1 - γ Winkelkorrelation der Reaktion $^{24}\text{Mg}(\alpha, \alpha_1\gamma)$ untersucht. Für 126 Winkelpaare wurden mit einer Mehrdetektor-Anordnung (4 Si(Li)-Teilchendetektoren und 2 Ge(Li) γ -Detektoren) die doppelt-differentiellen Wirkungsquerschnitte gemessen. Rechnungen mit der Methode der gekoppelten Kanäle auf der Basis des Rotationsmodells beschreiben die Korrelationsdaten recht gut. Es wurde eine große Empfindlichkeit auf das Vorzeichen der Quadrupoldeformation beobachtet, weitgehend unabhängig von der Wahl der Parameterwerte des optischen Potentials. Die beobachteten Prolate-Oblate-Effekte lassen sich im Rahmen eines einfachen Diffraktionsmodells verstehen.

1. Introduction

As demonstrated by various investigations ¹⁻³⁾ measurements of particle- γ angular correlations on nuclear reactions provide sensitive experimental tests of important features of the current reaction models. Results of $(\alpha, \alpha' \gamma)$ correlation experiments on even-even nuclei are of particular interest because in this case the individual reaction amplitudes leading to the magnetic substates of the excited residual state can be determined separately. The sensitivity of these amplitudes to some important parameters of the reaction model was already pointed out in ref. ⁴⁾.

In a previous letter ⁵⁾ we reported $(\alpha, \alpha_1 \gamma)$ angular correlation measurements on ^{24}Mg at a bombarding energy of 104 MeV. The correlation data were analysed in terms of coupled channels on the basis of the symmetric rotator model. The analyses resulted in a very good agreement between the experimental quantities and model calculations based on the conventional extended optical model (EOM). The correlation data, especially the amplitude of the correlation function, were found to be very sensitive to the sign of the intrinsic quadrupole deformation of the target nucleus. The remarkable prolate-oblate effects turned out to be nearly insensitive to the used optical model parameters.

In the present work we present some more details of the experiment and report on the results of a more extended analysis on the basis of a semi-microscopic folding model allowing a direct comparison to electron scattering results. Furthermore we attempt to explain the characteristic features of the distinct prolate oblate effects in the framework of Blair's diffraction model.

Submitted: 25.4.1977

2. Experiment and data evaluation

2.1. Beam handling and monitoring

The measurements have been performed with the 104 MeV α -particle beam at the Karlsruhe isochronous cyclotron. The beam energy spread was about 300 - 400 keV. One of the main experimental problems was the considerable γ -background radiation due to the high bombarding energy. In order to minimize the background radiation the beam has been guided to the target without any slits, and we have not used the external beam analysing system in order to avoid slit reactions. The position and the profile of the beam has been monitored during the experiment by a ZnS-screen mounted behind the Faraday cup. Periodical observations of the beam spot on this screen by use of a TV camera - for this purpose the Faraday cup had to be removed shortly - showed a very stable position of the beam spot. A control still more sensitive than this optical observation proved to be the counting rates of the Ge(Li)-detectors: optimal focussing yielded a sharp minimum of these counting rates.

2.2. The scattering chamber and detectors

In fig. 1 the experimental setup is shown schematically. For the measurement of the α - γ angular correlations a scattering chamber with a diameter of 45 cm was used. The dimensions of the scattering chamber are a compromise between the requirements of high angular resolution together with an exact definition of the particle scattering angles and, on the other hand, detection efficiency and solid angles as large as possible for the γ -detectors. For the detection of the scattered α -particles four Si(Li) detectors with an active area of about 300 mm² have been used. Rectangular slits in front of the detector with a width of 2.5 mm in a distance of 15 cm from the

target yield an angular resolution of about 0.5° and a solid angle of about $1.5 \cdot 10^{-3}$ sr. In order to improve the timing behaviour of the Si(Li) detectors, they have been cooled down to -70° C. Two additional Si(Li) detectors served as monitor counters. The γ -quants were detected with two Ge(Li) detectors having an active volume of about 45 cm^3 . In an experimental comparison Ge(Li) detectors turned out to be superior to NaI detectors. The smaller efficiency of the Ge(Li) detectors is counterbalanced by the higher energy resolution and first above all by the stability of the gain against fluctuations of the counting rates. The Ge(Li) detectors were coated with lead collimators with a thickness of about 10 cm, which could be moved outside around the reaction chamber in the reaction plane. The front of both γ detectors was shielded with a layer of lead of 5 mm. By this way the number of low-energetic γ -rays could be kept relatively small so that higher counting rates in the region of higher γ -energies could be processed. The target was a foil of ^{24}Mg (isotopically enriched $> 99.9 \%$) of a thickness of 6 mg/cm^2 .

2.3. Electronics and data acquisition

The set-up of the electronics is displayed by the block diagram in fig. 2. The output signals of the charge sensitive preamplifiers (PA) are split into energy and time branches. Due to the relative large rise times for the derivation of the time marking signals for both the γ detectors and the particle detectors the method of constant fraction of pulse height triggering (CFT) is used. The time signals from the particle detectors were tuned against another by delays (D), mixed and given onto the start signal of two time-to-pulse-height-converters (TPC) which are stopped by the delayed time signals of the Ge(Li) detectors. Fig. 3 shows a typical TPC-

spectrum with the coincidence peak situated on a relative high background. The periodic structure reflects the time distance of the cyclotron bursts. The time resolution ($t_{1/2} \approx 15$ ns) of the coincidence peak is smaller than the period of $t_z = 30$ ns of the cyclotron. Single channel analyzers (SA) selecting the events within the coincidence peak open linear gates (LG), the analog inputs of which are fed with the suitably shaped and delayed energy signals of the particle and γ detectors. This part of the electronics is similar to that described in detail in ref. 6). Subsequently windows are set on the α_1 -peaks of the biased (BA) α -particle spectra by single channel analyzers. By their output signals additional linear gates are opened, which are fed by γ -signals fulfilling the first coincidence requirement (given by the TPC-window). The γ -spectra obtained by this way are analysed by a routed multichannel analyzer. For comparison fig. 4 shows for one of the Ge(Li) detectors the "free" γ -spectrum, the γ -spectrum after the first coincidence requirement (in coincidence with all α -spectra) and the γ -spectrum after the second coincidence requirement (in coincidence with the α_1 -peak of one particle spectrum). In order to determine the contribution of random coincidences for both Ge(Li) detectors one spectrum (randomly) coincident with the α_0 -peak has been analysed. The ratio of the random to true coincidences in the other spectra has been obtained by multiplying measured coincident counting rate with the corresponding ratio of α_0 -peak to α_1 -peak. Additionally the relative part of random coincidences has been determined independently by evaluating the suppression of the 511 keV background line. The ratio of random to true coincidences was in general less than 10 %, at extreme forward angles of the particle detectors up to 30 %.

All critical points of the electronics have been controlled either continuously or in certain time intervals especially to recognize shifts of the electronic "windows" as soon as possible.

2.4. Angular correlation function and reaction amplitudes

The double differential cross section of a reaction $A(a,b) B(\gamma)C$ can be written as

$$\frac{d^2\sigma}{d\Omega_b d\Omega_\gamma} = \frac{1}{4\pi} \frac{\Gamma_{\gamma C}^B}{\Gamma_B} W(\theta_b, \phi_b; \theta_\gamma, \phi_\gamma) \cdot \frac{d\sigma}{d\Omega_b} \quad (2.4.1)$$

There $\frac{\Gamma_{\gamma C}^B}{\Gamma_B}$ is the branching of the γ -decay of the state B to the state C, W is the angular correlation function, which depends on the angles of the observed emitted particle b and of the observed γ -quantum. In ref. ⁷⁾ a general expression is given for the angular correlation function in dependence on the reaction amplitudes $X_{m_a M_A m_b M_B}$ between the magnetic substates of the entrance and the exit channel. In the special case of $(\alpha, \alpha' \gamma)$ angular correlations with a spin sequence $J_A = 0 \rightarrow J_B = 2 \rightarrow J_C = 0$ the individual reaction amplitudes can be determined as is described e.g. in ref. ¹⁾. With the axis of quantization chosen in the direction of $\underline{k}_a \times \underline{k}_b$, the "in-plane" angular correlation function has the form

$$W(\theta_\alpha = \frac{\pi}{2}; \phi_\alpha; \theta_\gamma = \frac{\pi}{2}; \phi_\gamma) = A + C \sin^2 2(\phi_\gamma - \phi_2) \quad (2.4.2)$$

which can be expressed by the reaction amplitudes

$$X_{\pm 2} = |X_{\pm 2}| \cdot e^{-i 4\gamma_{\pm 2}}$$

as

$$W(\theta_\alpha = \frac{\pi}{2}; \phi_\alpha; \theta_\gamma = \frac{\pi}{2}; \phi_\gamma) = \frac{5}{4} ((|X_2| - |X_{-2}|)^2 + 4|X_2| |X_{-2}| \cdot \sin^2 2 \cdot (\phi_\gamma - (\gamma_{-2} - \gamma_{+2}))) \frac{1}{\frac{d\sigma}{d\Omega_\alpha}} \quad (2.4.3)$$

Thus from the "in-plane" angular correlation function the amplitudes $|X_{+2}|$, $|X_{-2}|$ and their relative phase ($\gamma_{-2} - \gamma_{+2}$) can be determined in dependence of the α -scattering angle. Due to Bohr's theorem ⁸⁾ the amplitudes X_{+1} and X_{-1} are zero. As the amplitudes $|X_{+2}|$ and $|X_{-2}|$ in the angular correlation function enter symmetrically, a discrimination between both is impossible without a measurement of the sign of the circular polarization of the γ -radiation. The absolute value of the amplitude X_0 however follows uniquely from the differential cross section

$$\frac{d\sigma}{d\Omega_\alpha} = |X_{-2}|^2 + |X_0|^2 + |X_{+2}|^2 \quad (2.4.4)$$

The relative phase of X_0 can be determined with the aid of an "out-of-plane" correlation measurement. In the present work we omitted this measurement as there is no indication that this phase is expected to be more sensitive to the features of the used models and their parameters than the quantities extracted from "in plane" measurements.

Sometimes it proves to be more convenient to consider the quantities A and C (see e.g. 2.4.2) which are combinations of the reaction amplitudes X_{M_B} rather than the isolated reaction amplitudes themselves. As in our case A equals to zero, C is given by

$$C = \frac{5}{2 + \frac{|X_0|^2}{|X_2|^2}} \quad (2.4.5)$$

Some sensitivities of the amplitudes X_0 and X_2 , which may be cancelled in the differential cross section, may be enlarged in the magnitude C depending on the ratio X_0 to X_2 .

In the present work double differential cross sections $\frac{d^2\sigma}{d\Omega_\alpha d\Omega_\gamma}$ of the $^{24}\text{Mg}(\alpha, \alpha_1\gamma)^{24}\text{Mg}$ angular correlation have been determined in the reaction plane for 21 particle angles from $6,5^\circ \leq \phi_{\alpha,lab} \leq 35^\circ$ for always six positions of the γ -detectors.

To exclude systematic errors as far as possible following up each coincidence run the differential cross section has been determined.

The angular correlation function was finally obtained from

$$W = \frac{4\pi}{\epsilon_\gamma d\Omega_\gamma} \cdot \frac{N_{\text{coi}}}{N} \cdot \frac{j}{j_{\text{coi}}} \quad (2.5.6)$$

- with $\epsilon_\gamma d\Omega_\gamma$: product of absolute photopeak efficiency and solid angle of the γ -detector
- N_{coi} : number of coincidence events in the photopeak of the γ spectrum
- N : number of the events in the α_1 peak of the free particle spectrum
- j_{coi} : number of incoming particles in the coincidence measurement
- j : number of incoming particles in the free measurement

By this procedure errors in the determination of solid angles of the particle detectors, of the absolute measurement of the current and the target thickness and discrepancies of the particle scattering angles between single and double differential cross section are eliminated.

Fig. 5 shows as an example the experimental angular correlation function for the particle angle $\phi_{\alpha,lab} = 15.5^\circ$ as function of the angle of the γ detector. By a least squares fit the uncorrected quantities A' , C'

and ϕ_2 , have been determined. After a finite angle correction for the γ detector as described in ref. 9) the quantities A, C and ϕ_2 were obtained. In the present case the correction turned out to be very small. For the determination of the absolute values of the reaction amplitudes X_{MB} the differential cross section has been measured additionally with the analysed beam of the cyclotron in a large (135 cm \emptyset) scattering chamber. Details about the scattering facility are given in ref. 10).

3. Analysis and discussion

The EOM analyses of ref. ⁵⁾ have shown that the correlation amplitude C is very sensitive to the sign of the quadrupole deformation, but nearly independent of the used parameters of the optical model potential. Experimentally it has been found that the nuclear polarization A is zero within the statistical errors for all measured particle angles. Therefore for the determination of the experimental absolute squares of the reaction amplitudes, the quantity A was set equal 0 with the consequence that $|X_{+2}|_{\text{exp}}^2 = |X_{-2}|_{\text{exp}}^2$. This agrees with the results of the coupled channels calculations which predict very small values for A (10^{-2} to 10^{-3}). In fig. 6 supplementary to ref. ⁵⁾ the experimental absolute squares of the reaction amplitudes X_0 and $X_{\pm 2}$ are compared with EOM coupled channels calculations. The parameters (table 1 from ref. ⁵⁾) are the "best-fit" sets for prolate (drawn curve) and oblate (dashed curve) deformation. It is obvious, that also for the reaction amplitudes only the calculation with $\beta_2 > 0$ can reproduce the experimental data. Moreover one can see that the calculations for $\beta_2 > 0$ as well as for $\beta_2 < 0$ give very similar values for $|X_{+2}|^2$ and $|X_{-2}|^2$ i.e. that nearly no nuclear polarization occurs over the whole angular region.

Coupled channel analyses, in which the coupling potentials are obtained in the framework of the EOM, provide deformation parameters, which are related to the optical potential and not to the nuclear matter distribution. As a consequence of the short range of the nuclear forces it seems true that the shape of the optical potential follows the nuclear density distribution; in principle, however, the optical potential combines properties of the target nucleus and the projectile and does not represent the target nucleus alone. Therefore deformation parameters extracted from EOM analyses cannot be com-

pared directly with the results of other experiments, for instance with electron scattering data. Indeed for a long time there were discrepancies between the absolute values of the deformation parameters extracted by various methods ^{*}).

Recently a simple folding model approach has been applied successfully to elastic and inelastic α -particle scattering ¹¹⁾. A comprehensive review on this model is given in ref. ¹²⁾. There is the interesting question, whether this folding model provides an equivalent and sufficiently good description of α - γ angular correlation data. The folding model generates the real part U_R of the optical potential by a folding of the target density ρ_m with an effective projectile-bound nucleon interaction V_{eff} . Thus, the expression defining the model for the elastic scattering is:

$$U_R(\vec{r}_\alpha) = \int V_{\text{eff}}(\vec{r}_\alpha, \vec{r}) \rho_m(\vec{r}) d^3\vec{r} \quad (3.1)$$

with

$$\rho_m = \left\langle 0 \left| \sum_{i=1}^A \delta(\vec{r} - \vec{r}_i) \right| 0 \right\rangle$$

For the effective projectile-nucleon interaction a simple Gaussian form

$$V_{\text{eff}} = \lambda_R(E) V_0 \exp(-|\vec{r} - \vec{r}_\alpha|^2 / \mu_0^2) \quad (3.2)$$

is chosen ¹³⁾ whose range μ_0 takes into account the finite size of the projectile. The energy-dependent factor $\lambda_R(E)$ absorbs a correction of the free α -nucleon interaction due to the bound target nucleons.

^{*}) It should be noted that $(\alpha, \alpha'\gamma)$ angular correlation data are very sensitive to the sign of the deformation parameters, while their absolute values are fixed already from the differential cross sections.

In the description of inelastic scattering the real part of the coupling potential for the nuclear excitation is derived by folding V_{eff} analogously into the transition densities

$$\rho_{n \rightarrow n'} = \langle n' | \sum_{i=1}^A \delta(\vec{r} - \vec{r}_i) | n \rangle. \quad (3.3)$$

In the phenomenological procedure of the collective model the transition densities are derived from a Fermi shape

$$\rho_m(\vec{r}) = \rho_0 / (1 + \exp [(r - c_m] / a_m)), \quad (3.4)$$

dynamically or permanently deformed by an angular dependence of $c_m = c_m(\hat{r})$. For the imaginary part of the optical potential the standard Saxon-Woods representation is usually used.

The present folding model analyses are based on a rotational model description of ^{24}Mg , and the calculations have been done in a $0^+ - 2^+ - 4^+$ coupling scheme. For the calculations we used a modified version of the code ECIS¹⁴⁾ (including a routine for an adequate presentation of the reaction amplitudes¹⁵⁾ *). First of all the matter density distribution was fixed by the values from electron scattering experiments¹⁷⁾. The parameters of a Fermi distribution obtained from electron scattering data have to be corrected due to the finite size of the protons within the nucleus as described in ref.¹⁸⁾. The parameter values modified in this way have then been used to generate the real part of the optical potential. With this potential we started to fit the differential cross sections of the elastic and inelastic scattering in the total region $6.5^\circ \leq \theta_\alpha \leq 45^\circ$. However,

*) For calculations with the EOM we also used the code INCH1¹⁶⁾.

neither with the assumption of $\beta_2 > 0$, not with $\beta_2 < 0$ we could achieve satisfactory agreement with the experimental data. But the fits could be improved remarkably by considering only the scattering angles $\phi_\alpha \leq 30^\circ$. The final parameter values of these fits are given in table 1. In fig. 7 the fits are displayed together with the experimental data. Both fits can reproduce the elastic as well as the inelastic cross section favouring slightly the prolate deformation, which can be seen also from the χ^2 -values. For scattering angles $\phi_\alpha \geq 30^\circ$ the experimental values are underestimated by both calculations. This behaviour is generally observed in analyses with this folding model. The steeper slope of the predicted cross sections at larger angles is supposed to arise from the simplified form of the effective interaction and neglecting the antisymmetrization.^{12, 19)}

The deformation parameters resulting from the present fits are $\beta_2 = 0.47$ and $\beta_2 = -0.66$, respectively. These values are clearly greater than those resulting from the EOM analyses⁵⁾ ($\beta_2 = 0.34$ and $\beta_2 = -0.45$, respectively) expressing the quantitative difference between potential deformation extracted from EOM analyses and matter deformation extracted from folding model analyses. The parameters for $\beta_2 > 0$ in table 1 change only insignificantly compared to those of the electron scattering results¹⁷⁾. Especially the β_2 -value remains fixed at the electron scattering value of $\beta_2 = 0.47$.

Analysing the correlation data the folding model predicts - just as the EOM - very small values for the nuclear polarization A in the whole angular region in agreement with the experiment. The phase ϕ_2 has not been analysed in the framework of the folding model. The EOM analyses already showed that in comparison with the experimental errors the phase ϕ_2 is less affected by variations of potential and deformation parameters. This

is demonstrated in fig. 8 where the EOM calculations with the best fit parameters for prolate and oblate deformation are compared to the experimental values. The straight line is the adiabatic limit²⁰⁾. It differs only a little from results of the coupled channels calculations and seems to be able to describe the experimental data equivalently well.

Stimulated by the results of ref. 5) we focussed our view in the folding model analyses to the correlation parameter C and to the absolute squares of the transition amplitudes. In fig. 9 the experimental values of C are shown together with folding model calculations with the potential sets for $\beta_2 > 0$ and $\beta_2 < 0$ (table 1) which were not further adjusted to the correlation data. The drawn curve representing the prolate deformation is in very good agreement with the experimental values up to angles of 30° . For α -scattering angles $\phi_\alpha \gtrsim 30^\circ$ there occur deviations in the magnitude of the same type as in the cross sections. The dashed curve representing the oblate deformation cannot reproduce the experimental points. In large regions it disagrees in the magnitude as well as in the phase. In fig. 10 the absolute squares of the reaction amplitudes are compared with the calculations. For the determination of the experimental values again the quantity A was set equal to zero. The calculation corresponding to the prolate deformation provides very good agreement also in this case up to 30° , whereas the calculation corresponding to oblate deformation does not match the data, in particular between 15° and 25° . For angles $\phi_\alpha \gtrsim 30^\circ$ the model gives essentially smaller values than the experiment for the amplitudes $|X_{+2}|$ and $|X_{-2}|$ for both signs of the quadrupole deformation. The agreement in the amplitude $|X_0|$, however, is considerably better.

Just as in the previous EOM analyses⁵⁾ in the folding model analyses the optical potential parameters have been varied extensively. The characteristic

differences between prolate and oblate deformation proved to be independent of the potential parameters also in this case thus confirming our conclusions of ref. ⁵⁾ that α - γ angular correlations provide a sensitive tool to determine the sign of quadrupole deformations.

The shape of the matter distribution in ^{24}Mg extracted from α -scattering data using the folding model is now in good quantitative agreement with results from the electron scattering data ¹⁷⁾ emphasizing that the folding model provides a procedure for extracting deformation parameters from α -scattering data in a way comparable to electron scattering analyses.

4. Prolate-oblate effects of the correlation amplitude C in the framework of a simple diffraction model

An analytic justification of the sensitivity of the correlation parameter C on the sign of the quadrupole deformation in the framework of the coupled channels formalism seems to be very difficult. This is due to the complicated structure of the reaction amplitudes caused by the coupling of the radial equations and to the contribution of many partial waves. One can realize however that this sensitivity comes from the interference of single and multistep processes, which contribute to the reaction amplitudes in different orders of the deformation parameters. In the following section we attempt to point out the origin of the sensitivity of the amplitude C to the sign of β_2 by use of a refined diffraction model ²¹⁾. For this we extend previous similar considerations ^{22,23)} for the differential cross sections to angular correlation quantities where the prolate oblate effects are observed to be considerably increased. Recently prolate oblate effects in measured differential (α, α') cross sections have been analysed very extensively on the basis of diffraction models ²⁴⁾. The approximations of the diffraction models are expected to be reasonable for small scattering angles, and when bombarding energy is fairly large compared with the excitation energy and when strong absorption phenomena are dominating the scattering mechanism.

It is a well known fact, that a simple diffraction model succeeds at least in reproducing the diffraction pattern of the differential cross section. In the most simplest version one obtains analytic expressions for the reaction amplitudes, and therefore the interference effects between first and higher order terms should be rather transparent. Taking into account the terms up to second order, the reaction amplitudes for inelastic scattering

of spin zero particles from a state with spin I can be written as ²¹⁾

$$X_{I, M_I} = X_{I, M_I} (1) + X_{I, M_I} (2)$$

$$\text{with } X_{I, M_I} (1) = i k R_0 \cdot C_1(I) \cdot \left(\frac{2I+1}{4}\right)^{1/2} \cdot [I: M_I] \cdot J_{|M_I|}(x)$$

$$\text{and } X_{I, M_I} (2) = \frac{i k}{2} \cdot C_2(I) \cdot \left(\frac{2I+1}{4}\right)^{1/2} \cdot [I: M_I] \cdot \left[\left(1+x \frac{d}{dx}\right) J_{|M_I|}(x) \right] \\ + \frac{i k}{2} \Delta_{I, M_I} (-i)^{M_I} \cdot J_{|M_I|}(x)$$

$$\text{for } (M_I + I) \quad \text{even}$$

(4.1)

$$= 0 \text{ for } (M_I + I) \text{ odd}$$

where x is defined as the product of the radius R_0 of the nucleus, the momentum b of the projectile and the scattering angle θ : $x = k \cdot R_0 \cdot \theta$

J_{M_I} are spherical Bessel functions and

$$[I : M_I] = i^I \frac{[(I + M_I)! (I - M_I)!]^{1/2}}{(I + M_I)!! (I - M_I)!!} \quad (4.2)$$

In the reduced matrix elements of first and second order

$$C_1(I) = \frac{\beta_I \cdot R_0}{\sqrt{2I+1}} \text{ and } C_2(I) = \frac{\langle L 0 I 0 | L, 0 \rangle^2}{\sqrt{4\pi}} \cdot (\beta_L R_0)^2 \quad (4.3)$$

the β_L 's are the deformation parameters of the nucleus. In order to agree with the formulas in ref. ²¹⁾ the quantization axis is chosen in beam direction.

The second order contributions $X_{I, M_I}(2)$ contain terms Δ_{I, M_I} . The principal way to calculate them is shown in ref. ²¹⁾. In the special case of pure quadrupole deformation ($L = 2$) and inelastic scattering to a 2^+ -level ($I = 2$) which is of interest here a simple calculation yields:

$$\Delta_{2,2} = (R_0 \beta_2)^2 \cdot \frac{3 \cdot \sqrt{5}}{7 \cdot \sqrt{\pi}} \cdot \frac{\sqrt{6}}{4} \quad (4.4)$$

and

$$\Delta_{2,0} = (R_0 \beta_2)^2 \cdot \frac{3 \cdot \sqrt{5}}{7 \cdot \sqrt{\pi}} \cdot \frac{1}{2}$$

Thus the amplitudes in first order are proportional to β_2 , the second order contributions are proportional to β_2^2 . This is the origin of the dependence of the reaction amplitudes on the sign of the quadrupole deformation. As already shown e.g. in ref. ^{22,23)} different signs of β_2 lead to a slight phase shift in the diffraction pattern of the differential cross section similar to the result of coupled channels calculations. In the considerations of ref. ^{22,23)} the Δ_{I, M_I} terms in the second order contributions have been neglected.

The correlation amplitude C expressed by the reaction amplitudes is given by

$$C = 5 \cdot \frac{\left| \sqrt{\frac{3}{8}} - \frac{1}{2} \frac{X_2}{X_0} \right|^2}{1 + 2 \left| \frac{X_2}{X_0} \right|^2} \quad (4.5)$$

Including the second order terms, the ratio $\frac{X_2}{X_0}$ writes as

$$\frac{X_2}{X_0} = \sqrt{\frac{3}{2}} \cdot \frac{[(1-6\sqrt{\pi})\epsilon - 1] \cdot J_0(x) + \left\{ [1-(1-6\sqrt{\pi})\epsilon] \cdot \frac{2}{x} + \epsilon x \right\} J_1(x)}{[1 + (1 - 6\sqrt{\pi})\epsilon] J_0(x) - \epsilon x J_1(x)} \quad (4.6)$$

where ϵ is defined as $\epsilon := \sqrt{\frac{5}{\pi}} \cdot \frac{1}{14} \cdot \beta_2$

The upper part of fig. 11 demonstrates in which kind the correlation parameter C is affected by a change of the sign of the quadrupole deformation. For the deformation parameter β_2 the realistic value of $\beta_2 = \pm 0.4$ has been used. Drastic effects can be seen between the calculations with prolate (solid curve) and oblate (dashed curve) deformation. In the lower part of fig. 11 for comparison the results of extended optical model coupled channels calculations on the basis of the rigid rotator are displayed using the "best fit" parameter sets of the cross section analyses. It is obvious that the characteristic prolate-oblate effects which are present in the coupled channel predictions originate from features of the reaction mechanism which are described already by a simplified diffraction model.

Acknowledgements

We are indebted to Prof. Dr. G. Schatz and Dr. H. Schweickert for their encouraging interest and their efforts in adapting the technical conditions of the cyclotron operation to the specific requirements of our experiments. Furthermore we would like to thank the staff of the Karlsruhe cyclotron for good cooperation and Dr. H.J. Gils for some advice and help in using the CC code ECIS.

The work has been supported by the Deutsche Forschungsgemeinschaft and the Gesellschaft für Kernforschung m.b.H., Karlsruhe.

References

- 1) H. Wagner, A. Hofmann, and F. Vogler, Phys. Lett. 47B (1973) 497
- 2) W. Eyrich, S. Schneider, A. Hofmann, U. Scheib, and F. Vogler, Phys. Rev. C10 (1974) 2512
- 3) U. Scheib, A. Hofmann, and F. Vogler, Phys. Rev. Lett. 34 (1975) 1586
- 4) P.K. Glanz, and G.H. Rawitscher, Nucl. Phys. A217 (1973) 299
- 5) W. Eyrich, A. Hofmann, U. Scheib, S. Schneider, F. Vogler, and H. Rebel, Phys. Lett. 63B (1976) 406
- 6) W. Eyrich, A. Hofmann, U. Scheib, S. Schneider, and F. Vogler, Nucl. Inst. and Meth. 138 (1976) 543
- 7) F. Rybicki, T. Tamura, and G.R. Satchler, Nucl. Phys. A146 (1970) 659
- 8) A. Bohr, Nucl. Phys. 10 (1959) 486
- 9) H. Wagner, Dissertation, Erlangen 1974
- 10) H. Rebel, G.W. Schweimer, G. Schatz, J. Specht, R. Löhken, G. Hauser, D. Habs, and H. Klewe Nebenius, Nucl. Phys. A182 (1972) 145
- 11) H. Rebel and G.W. Schweimer, Z. Physik 262 (1973) 59
- 12) H. Rebel, Proceedings of the Internat. Summer School of Nucl. Phys. Predeal, Romania, Sept. 1974, ed. by A. Ciocănel - KFK Report 2065 (1974), and further references therein.
- 13) C.J. Batty, E. Friedman, and D.F. Jackson, Nucl. Phys. A175 (1971) 1
- 14) J. Raynal, and G.W. Schweimer, Modified version of the computer code ECIS, unpublished
- 15) G. W. Schweimer, private communication
- 16) A. Hill, Computercode INCH 1, Oxford 1967, unpublished
- 17) A. Nakada, and Y. Torizuka, J. Phys. Soc. Japan 32 (1972) 1
- 18) H. Gils, H. Rebel, G. Nowicki, A Ciocănel, D. Hartmann, H. Klewe-Nebenius, and K. Wisshak, J. Phys. G1 (1975) 343
- 19) I. Brissaud, B. Tatischeff, L. Bimbot, V. Comparat, A. Willis, and M. K. Brussel, Nucl. Phys. A191 (1972) 145

- 20) J. S. Blair, and L. Wilets, Phys. Rev. 121 (1961) 1493
- 21) N. Austern, and J.S. Blair, Ann. Phys. 33 (1965) 15
- 22) E.V. Inopin and A.V. Shebeko, JETP (Sov. Phys.) 24 (1967) 1189
- 23) H. Rebel, Nucl. Phys. A180 (1972) 332
- 24) A.V. Yushkov, Izvestiya Akad. Nauk SSSR. Ser. Fiz. 39(8) (1975) 1584,
and further references therein.

Appendix

Experimental reaction amplitudes X_{MB} of the $^{24}\text{Mg}(\alpha, \alpha_1)$ -scattering at 104 MeV bombarding energy extracted from α_1 - γ -angular correlations (quantization axis perpendicular to the reaction plane, CM-data)

alpha scattering angle $\theta_{\alpha, \text{CM}}$ (degree)	$ X_0 ^2$ mb/sr	$\Delta X_0 ^2$ mb/sr
8,5	102,00	8,84
10,8	24,30	1,98
11,5	16,63	1,45
14,0	12,32	0,86
16,0	21,42	3,60
18,3	19,50	1,80
19,5	10,08	1,76
20,0	7,02	0,54
20,5	5,40	0,68
21,5	4,32	0,50
23,3	5,34	0,54
24,8	5,98	0,68
26,0	5,88	1,58
27,5	5,02	1,04
28,5	4,28	1,08
29,5	3,64	0,46
30,8	3,32	0,32
34,0	4,34	0,44
35,0	4,32	0,86
37,0	3,02	0,80
39,0	4,10	0,32

alpha scattering angle $\theta_{\alpha,CM}$ (degree)	$ X_{+2} ^2 = X_{-2} ^2$ (mb/sr)	$\Delta X_{+2} ^2$ (mb/sr)
8,5	34,00	4,22
10,8	18,85	0,89
11,5	8,18	0,63
14,0	2,84	0,38
16,0	11,79	1,70
18,3	9,00	0,80
19,5	4,96	0,83
20,0	3,24	0,24
20,5	2,30	0,31
21,5	1,84	0,23
23,3	4,08	0,25
24,8	5,51	0,31
26,0	5,31	0,74
27,5	3,24	0,47
28,5	2,11	0,49
29,5	1,58	0,21
30,8	1,74	0,14
34,0	2,58	0,20
35,0	2,54	0,38
37,0	2,09	0,35
39,0	0,65	0,15

alpha scattering angle $\theta_{\alpha,CM}$ (degree)	Phase φ_2 (degree)	$\Delta\varphi_2$ (degree)
8,5	8,0	1,5
10,0	9,0	2,0
10,8	7,1	1,4
11,5	5,0	1,6
14,0	10,0	1,9
16,0	11,0	2,1
18,3	8,6	0,9
19,5	10,5	1,3
20,0	10,1	1,3
20,5	13,1	1,4
21,5	14,1	1,3
23,3	13,1	1,4
24,8	12,6	1,2
26,0	13,1	1,7
27,5	16,7	1,4
28,5	14,6	1,5
29,5	15,1	1,0
30,8	16,1	1,4
34,0	20,0	2,1
35,0	20,2	1,6
37,0	17,7	2,0
39,0	19,6	1,7

Figure captions

- Fig. 1: Experimental setup (schematically): 1: scattering chamber; 2: target; 3: Si(Li) detectors (movable); 4: monitor detectors; 5: slits; 6: Ge(Li) detectors; 7,8,9: lead shielding; 10: window for a TV-camera;
- Fig. 2: Block diagram of the electronics: G1,G2: γ detectors P1 - P4: particle detectors; PA: preamplifiers; TFA: timing filter amplifiers; CFT: constant fraction triggers; D: delay lines; TPC: time-to-pulse-height converters; SA: single channel analysers; A: amplifiers; PS: pulse stretchers; G: linear gates; BA: biased amplifiers; C1,C2: test points.
- Fig. 3: Spectrum of one of the time-to-pulse-height-converters (TPC).
- Fig. 4: upper part: "free" γ -spectrum
middle part: γ -spectrum of events which fulfill the first coincidence requirement
lower part: γ -spectrum of events which fulfill the first and second coincidence requirement
- Fig. 5: Experimental angular correlation function for a fixed particle scattering angle. The curve is a least-squares fit.
- Fig. 6: Experimental values of the squares of the reaction amplitudes of the reaction $^{24}\text{Mg}(\alpha, \alpha_1 \gamma)$ and coupled channels predictions on the basis of the extended optical model. The experimental values of $|X_{\pm 2}|^2$ have to be compared with the averaged values of the respective calculations for $|X_{+2}|^2$ and $|X_{-2}|^2$

- Fig. 7: Results of a coupled channels analysis of the $^{24}\text{Mg}(\alpha, \alpha')^{24}\text{Mg}$ differential cross sections on the basis of a semimicroscopic folding model.
- Fig. 8: Experimental results of the phase ϕ_2 , coupled channels predictions on the basis of the extended optical model and adiabatic limit.
- Fig. 9: Experimental results of the correlation parameter C and coupled channels predictions on the basis of a semimicroscopic folding model.
- Fig. 10: Experimental results of the squares of the reaction amplitudes and coupled channels predictions on the basis of a semimicroscopic folding model. The experimental values of $|x_{+2}|^2$ have to be compared with the averaged values of the respective calculations for $|x_{+2}|^2$ and $|x_{-2}|^2$.
- Fig. 11: Calculations of the correlation parameter C for prolate and oblate deformation in the framework of Blair's diffraction model (upper part) and in the framework of coupled channels on the basis of the extended optical model (lower part). (The singularities in the diffraction model calculations arising from the sharp cut-off approximation are smoothed out by the drawn curves.)

Table 1

	Best fit for $\beta_2 > 0$	Best fit for $\beta_2 < 0$
λ	0.99	0.99
V_0 (MeV)	37.0	37.0
μ_0 (fm)	2.0	2.0
a (fm)	0.42	0.37
C_0 (fm)	2.94	2.94
W (MeV)	25.3	15.9
r_i (fm)	1.58	1.58
a_i (fm)	0.60	0.79
β_2	0.47	-0.66
β_4	-0.03	-0.03
χ^2	4.4	8.7

Table caption

Table 1: Parameters used in the folding model procedure. The quantities C_0 , a , β_2 , β_4 represent a deformed Fermi shape used for the nuclear density distribution of ^{24}Mg . The quantities V_0 and μ_0 represent a Gaussian form for the effective α - ^{24}Mg interaction.

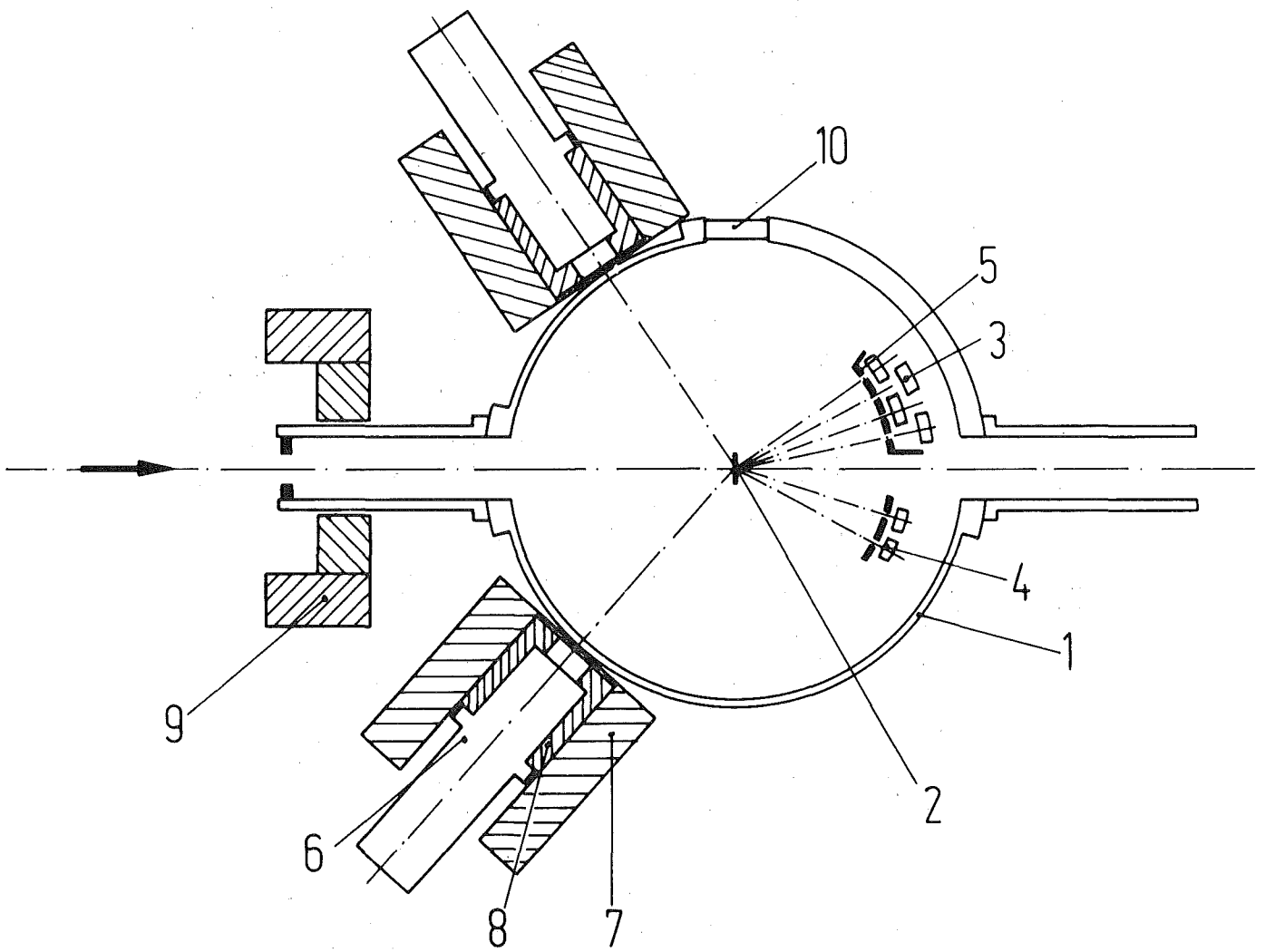


Fig. 1

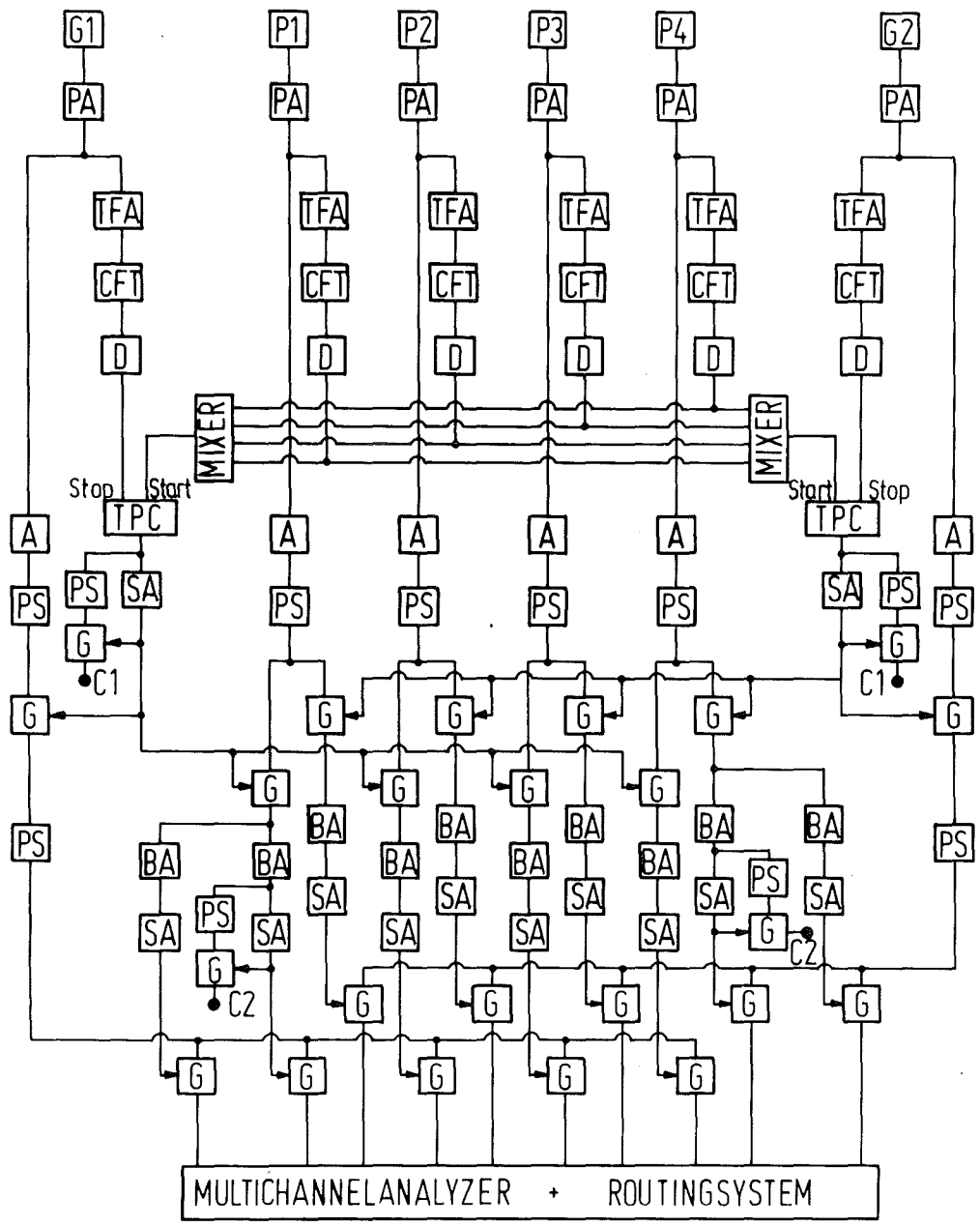


Fig. 2

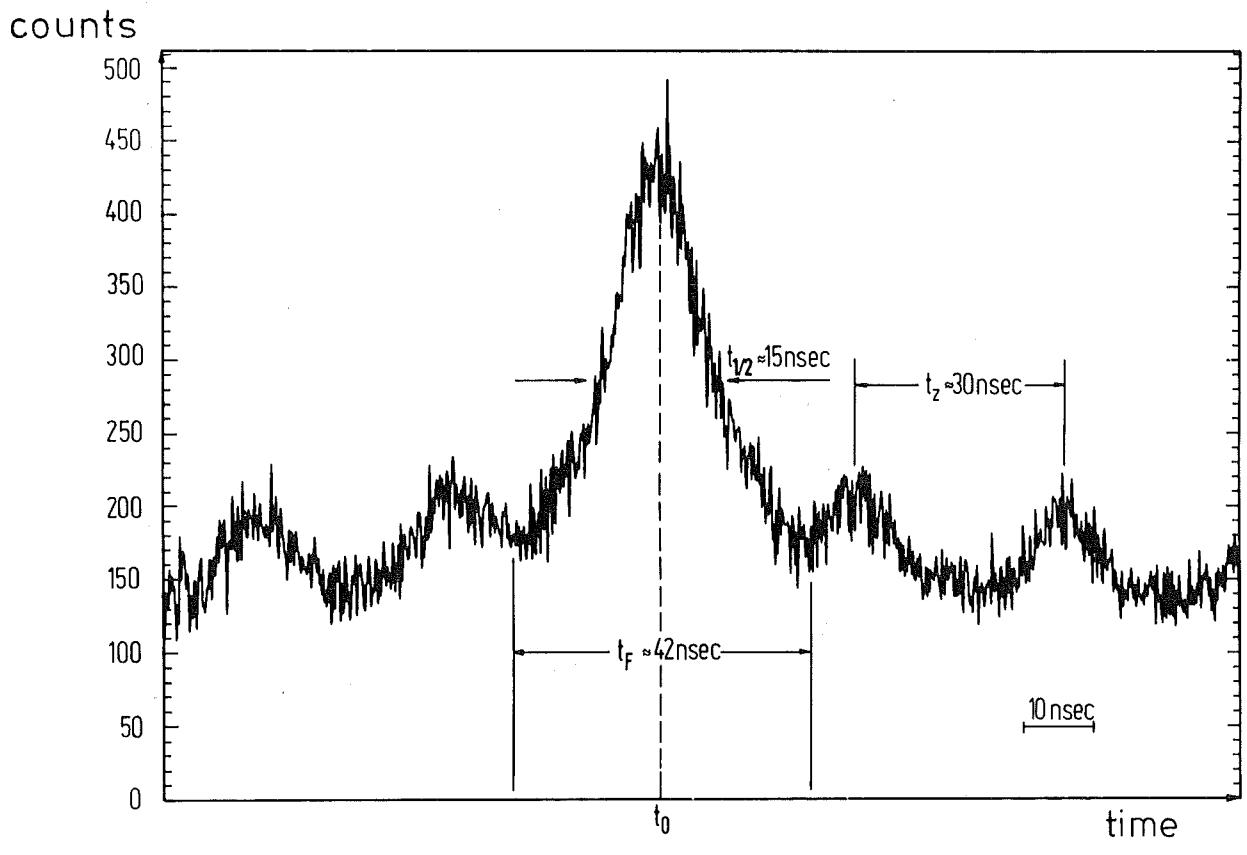


Fig. 3

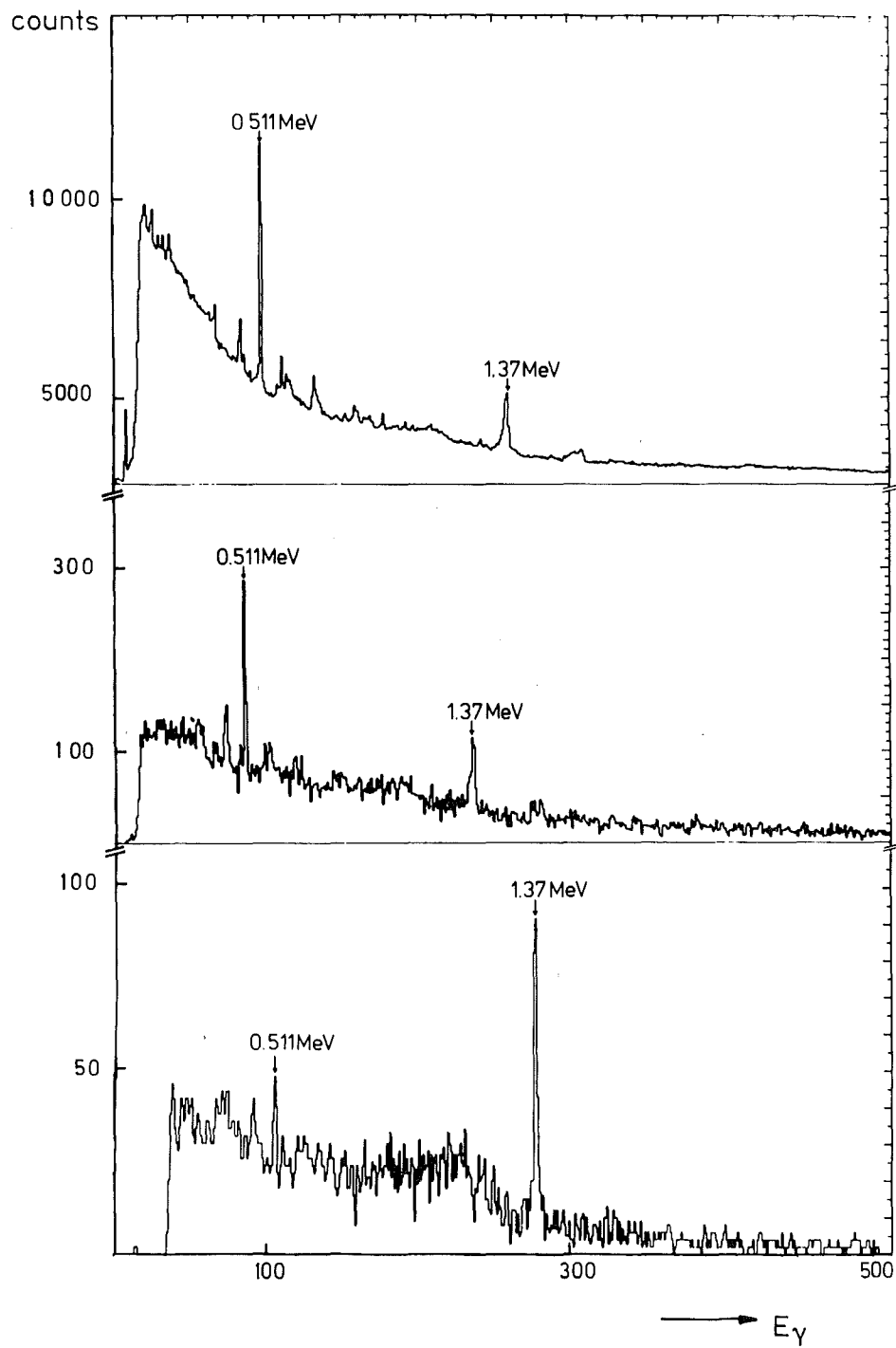


Fig. 4

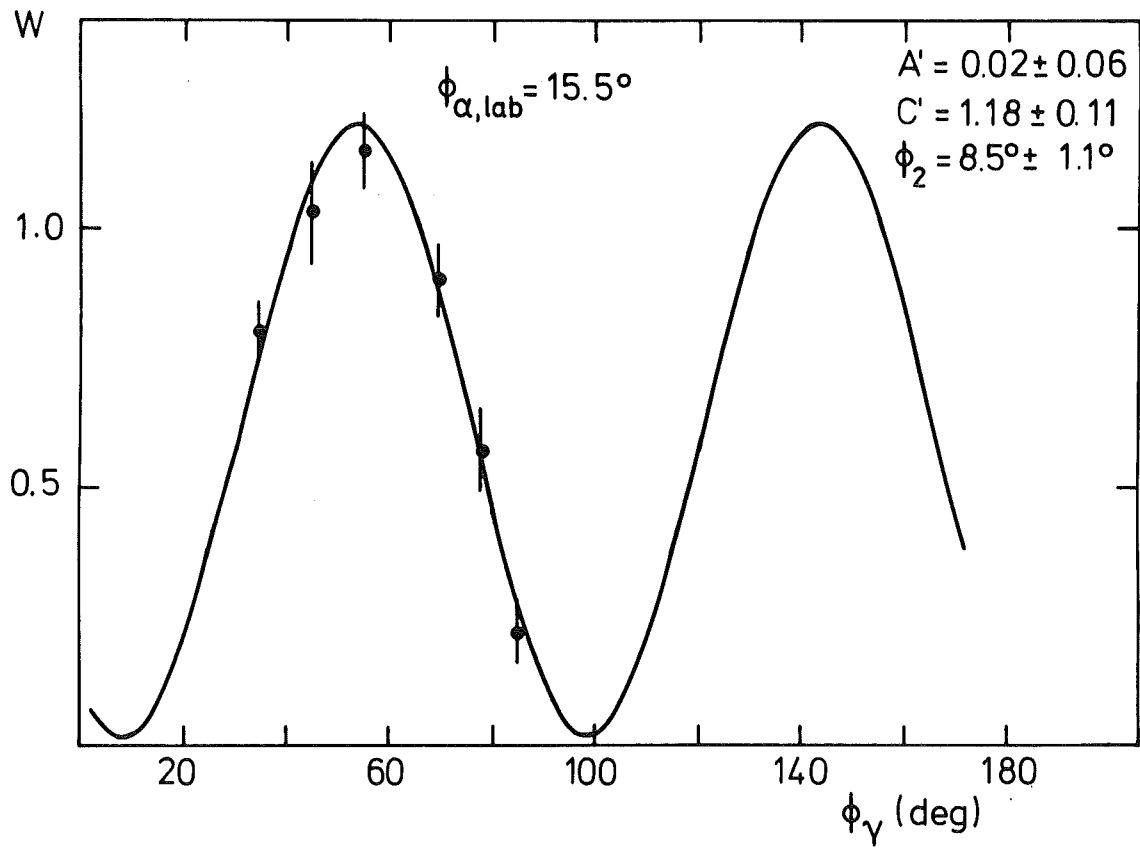


Fig. 5

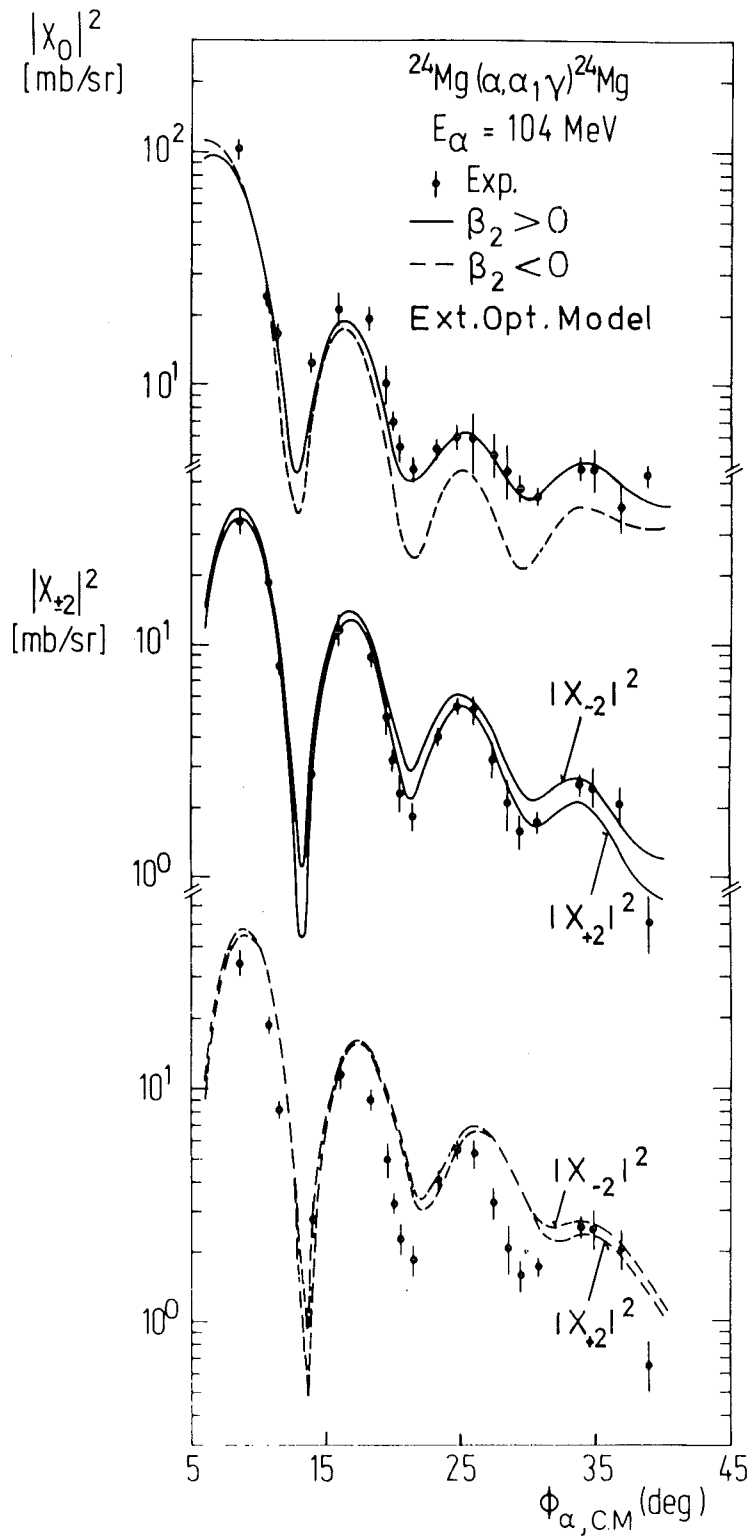


Fig. 6

$d\sigma/d\Omega$
[mb/sr]

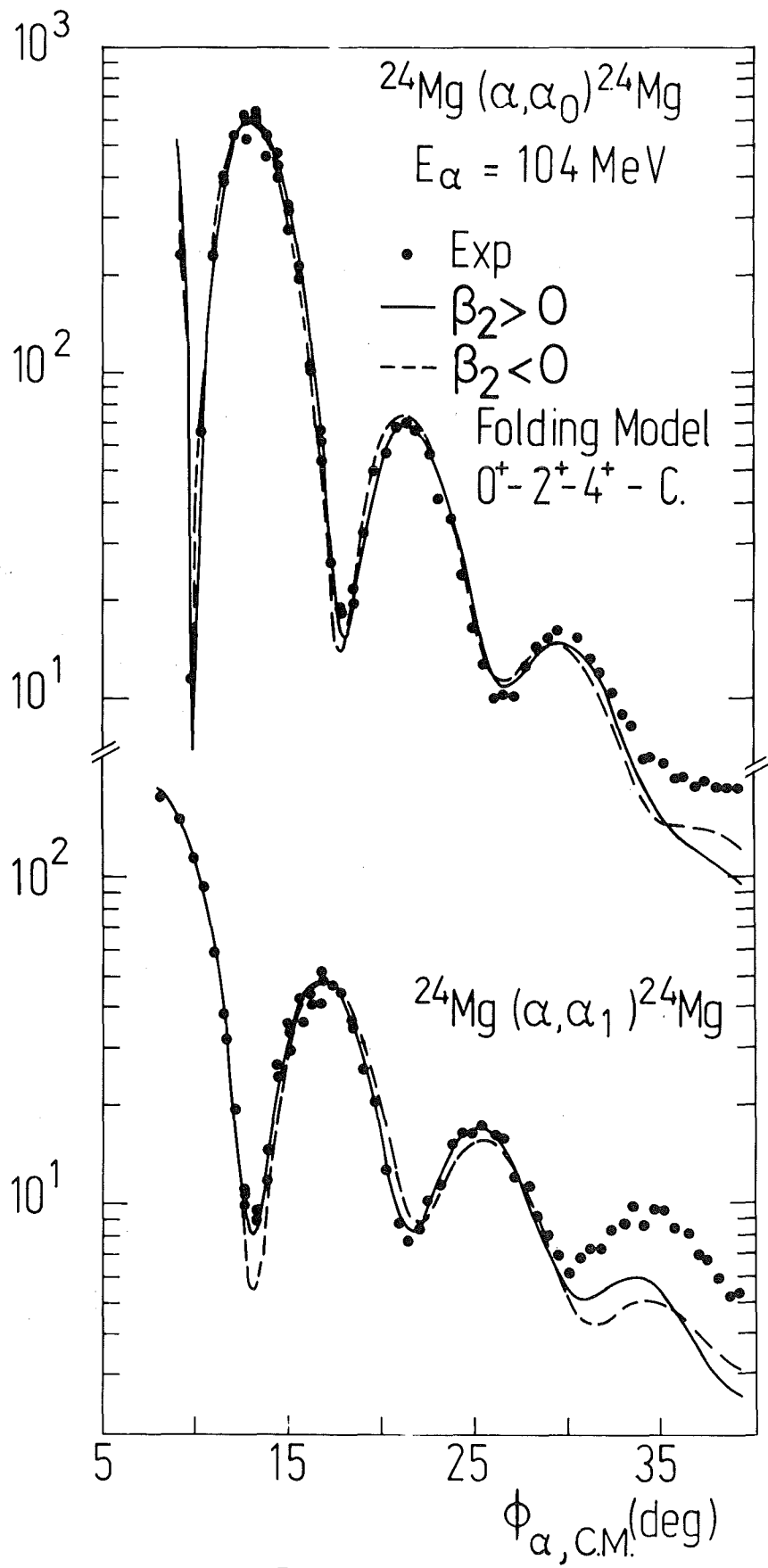


Fig. 7

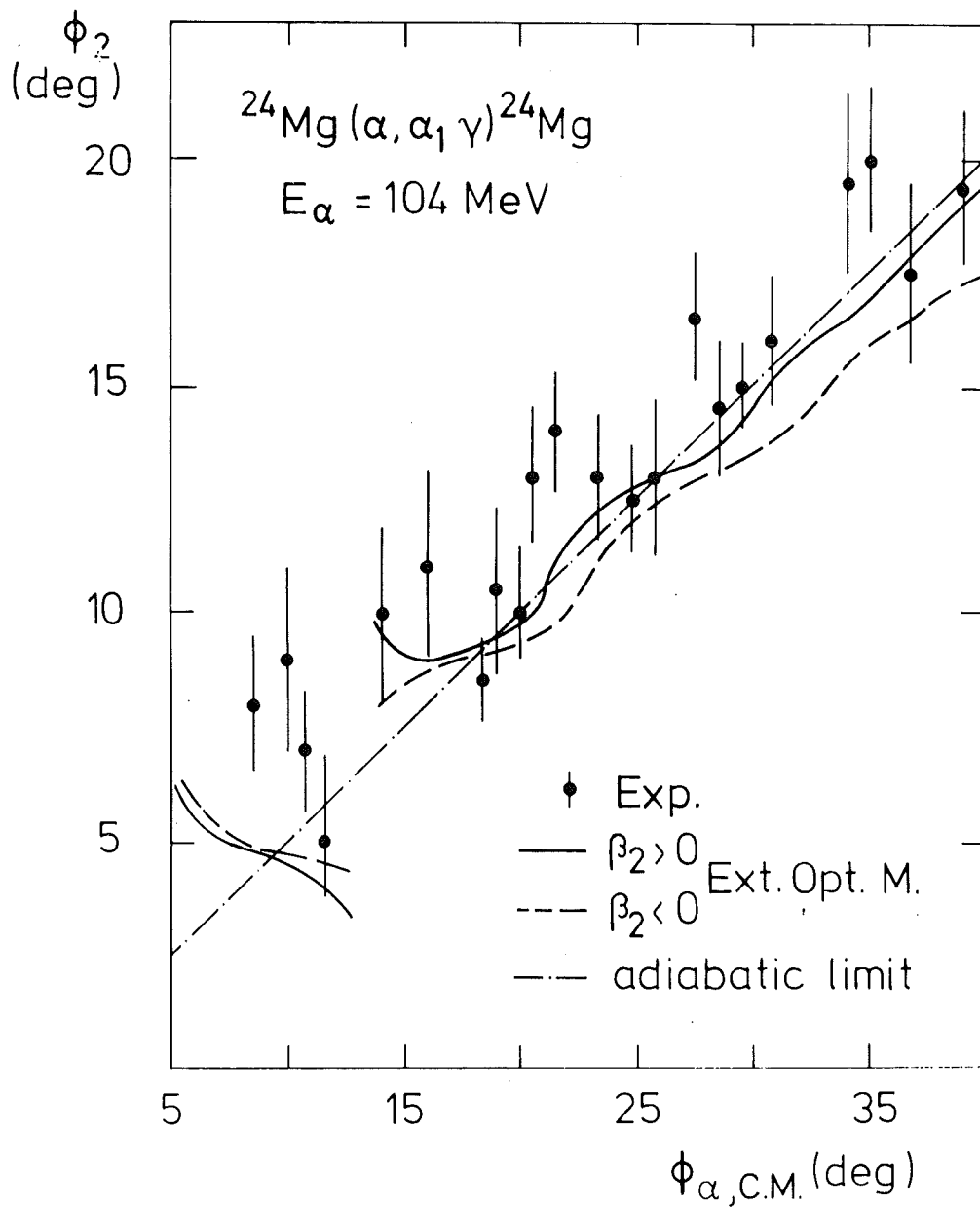


Fig. 8

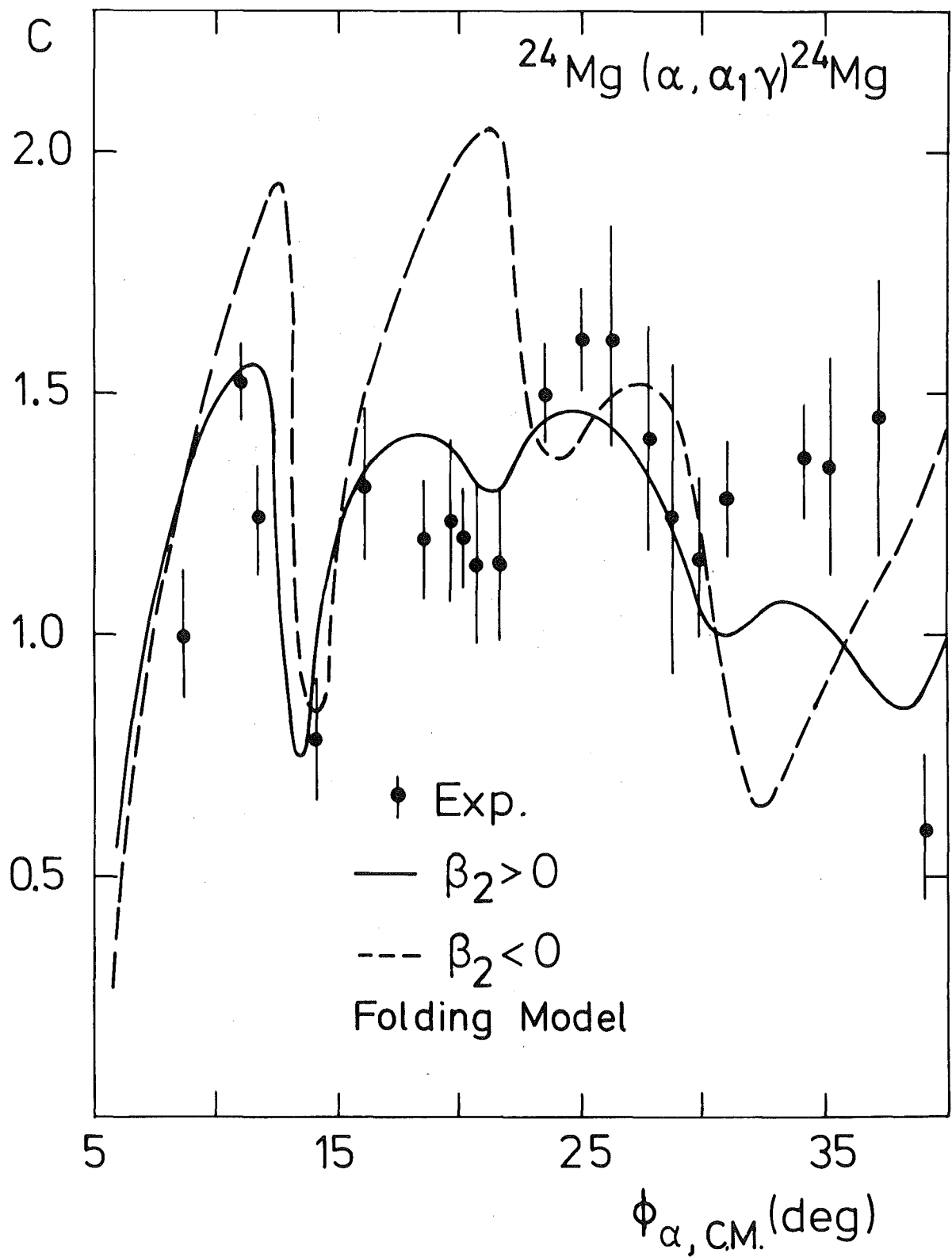


Fig. 9

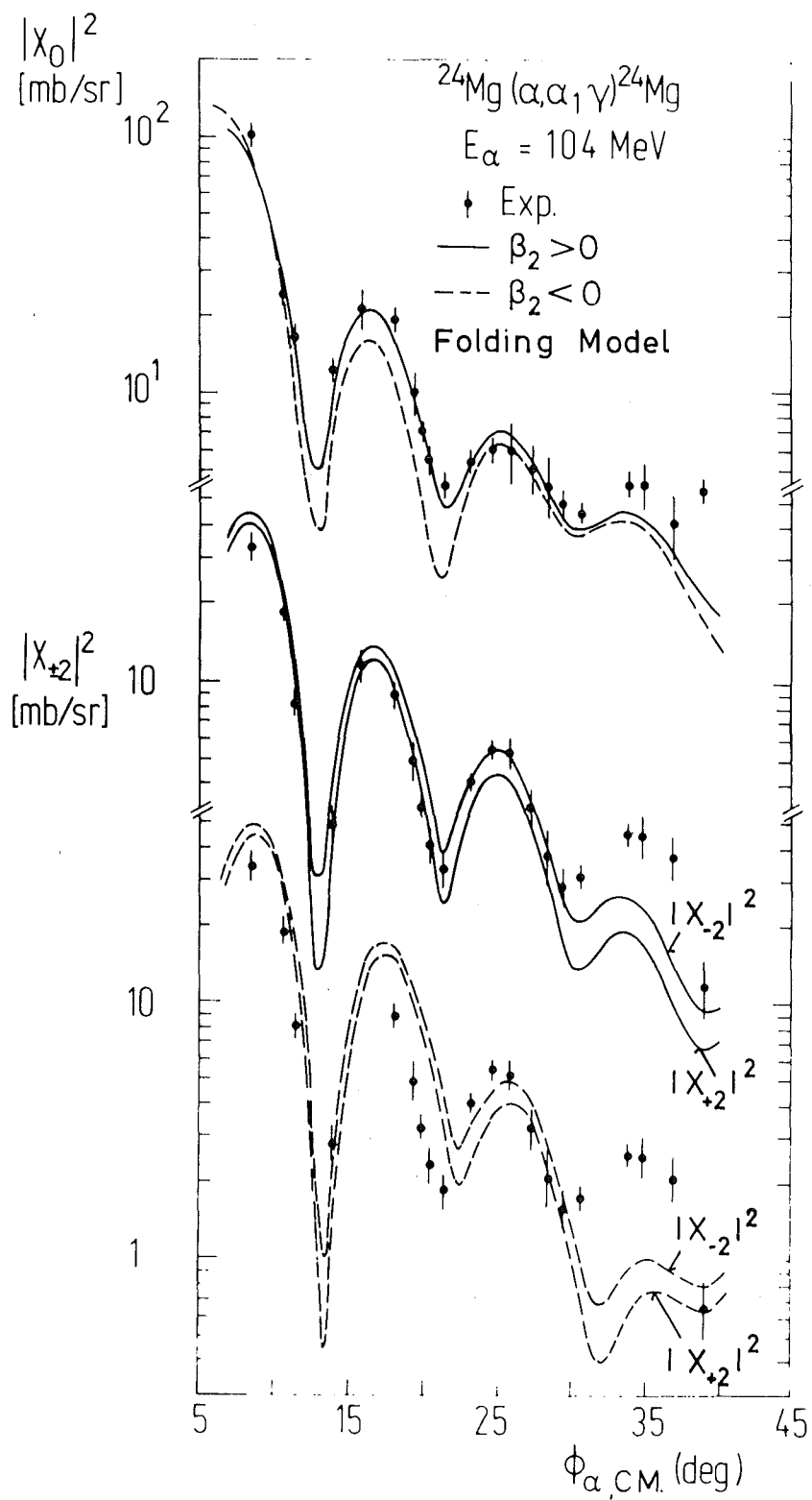


Fig. 10

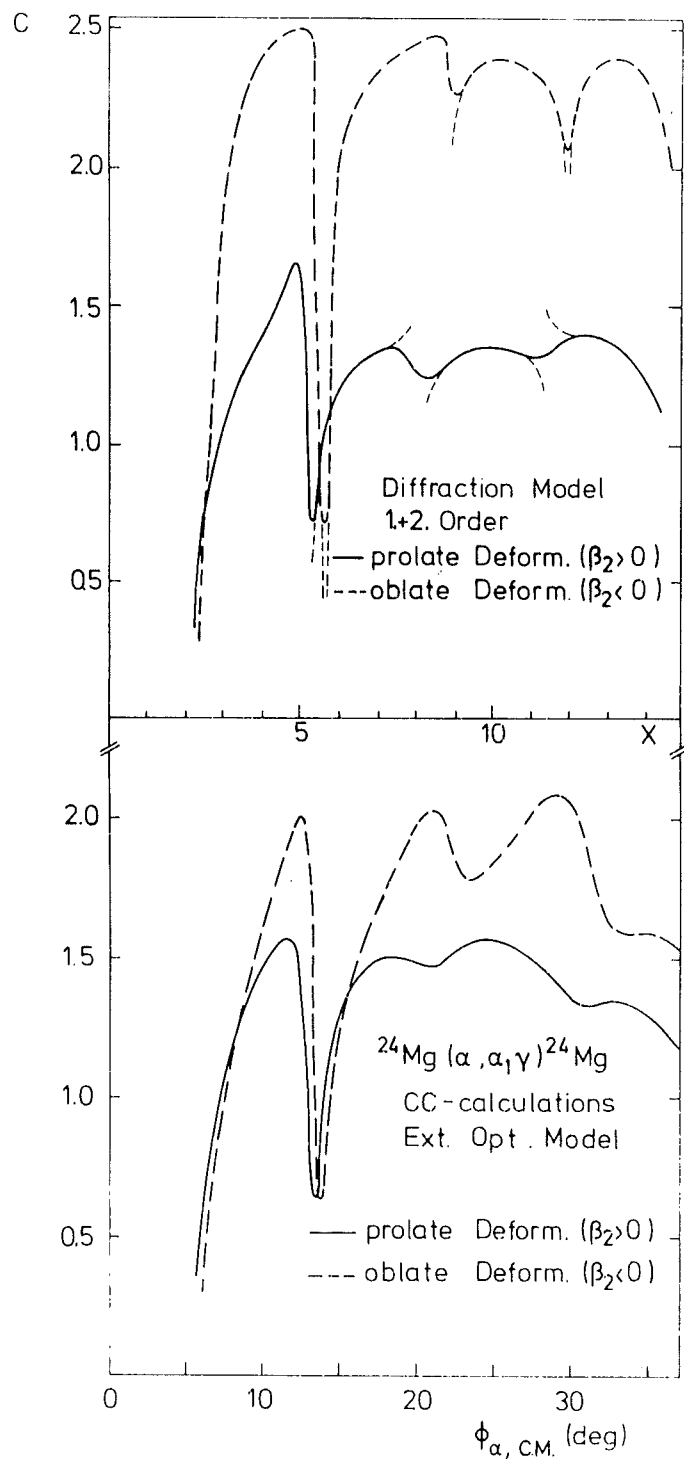


Fig. 11